

P-V-T equation of state of synthetic mirabilite ( $\text{Na}_2\text{SO}_4 \cdot 10\text{D}_2\text{O}$ )  
determined by powder neutron diffraction.

Supplementary Figures and Tables

A. D. Fortes<sup>1,2,\*</sup>, H. E. A. Brand<sup>3</sup>, L. Vočadlo<sup>1,2</sup>, A. Lindsay-Scott<sup>1,2</sup>,  
F. Fernandez-Alonso<sup>4,5</sup>, and I. G. Wood<sup>1,2</sup>

<sup>1</sup>*Centre for Planetary Sciences at UCL/Birkbeck, Gower Street, London WC1E 6BT, U.K.*

<sup>2</sup>*Department of Earth Sciences, University College London, Gower Street, London WC1E 6BT, U.K.*

<sup>3</sup>*Australian Synchrotron, 800 Blackburn Road, Clayton, VIC 3168, Australia.*

<sup>4</sup>*ISIS Facility, Rutherford Appleton Laboratory, Chilton, Didcot, Oxfordshire OX11 0QX, U.K.*

<sup>5</sup>*Department of Physics and Astronomy, University College London, Gower Street, London WC1E 6BT, U.K.*

\*corresponding author ([andrew.fortes@ucl.ac.uk](mailto:andrew.fortes@ucl.ac.uk))

## Figure S1

Pressure dependence of a) the  $a$ -axis, b) the  $b$ -axis, c) the  $c$ -axis, d) the monoclinic angle  $\beta$ , and e) the unit-cell volume of deuterated mirabilite on compression at 270 K; dashed lines are isothermal slices through the P-V-T BMEOS3 fitted to the observations. Uncertainties on all observations are smaller than the symbols, with the exception of d) where the error bars depict  $\pm 3\sigma$  uncertainties on  $\beta$ .

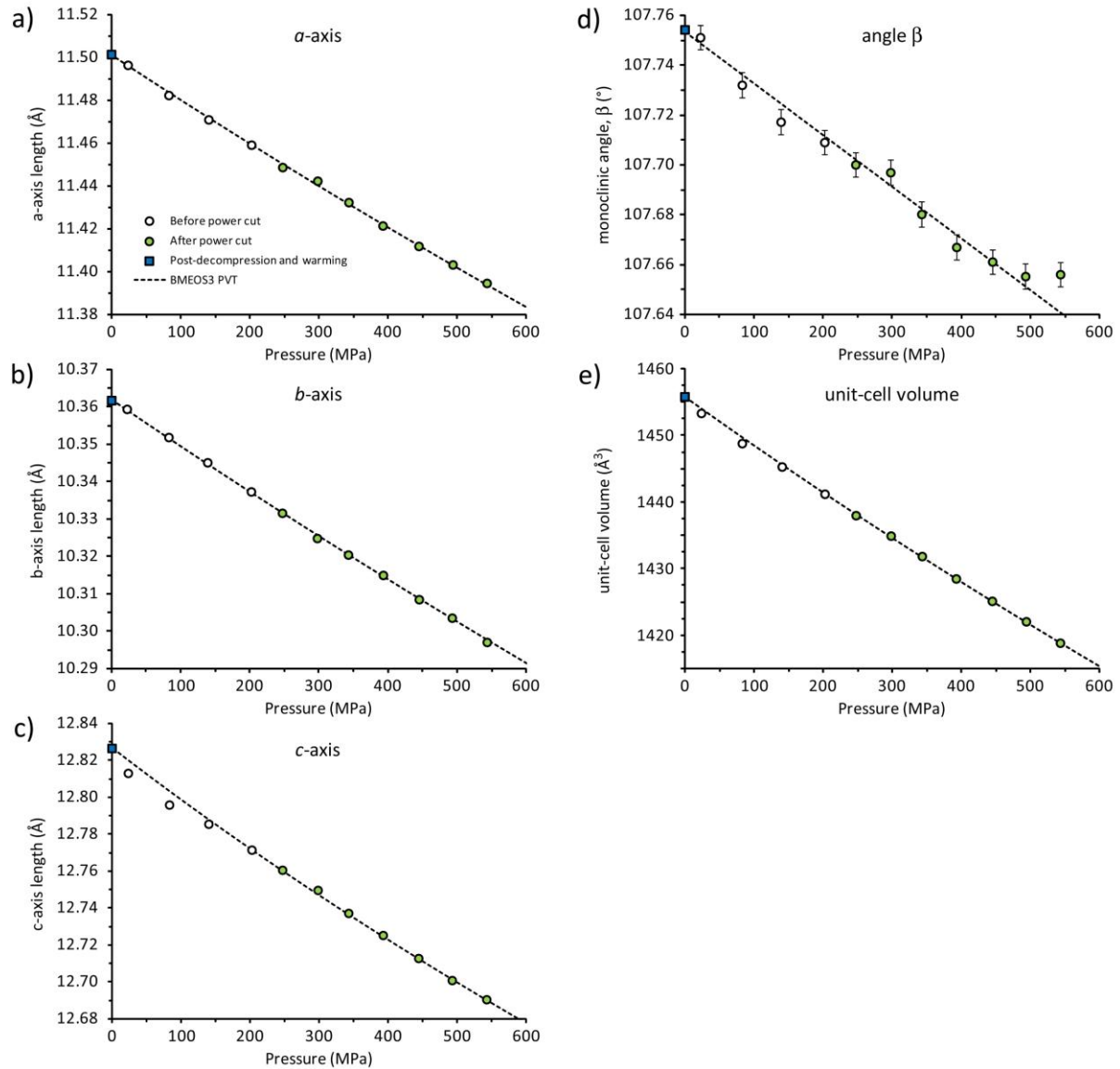


**Figure S2**

Temperature dependence of a) the  $a$ -axis, b) the  $b$ -axis, c) the  $c$ -axis, d) the monoclinic angle  $\beta$ , and e) the unit-cell volume of deuterated mirabilite on cooling at 543 MPa; dashed lines are isobaric slices through the P-V-T BMEOS3 fitted to the observations. Uncertainties on all observations are smaller than the symbols, with the exception of d) where the error bars depict  $\pm 3\sigma$  uncertainties on  $\beta$ .

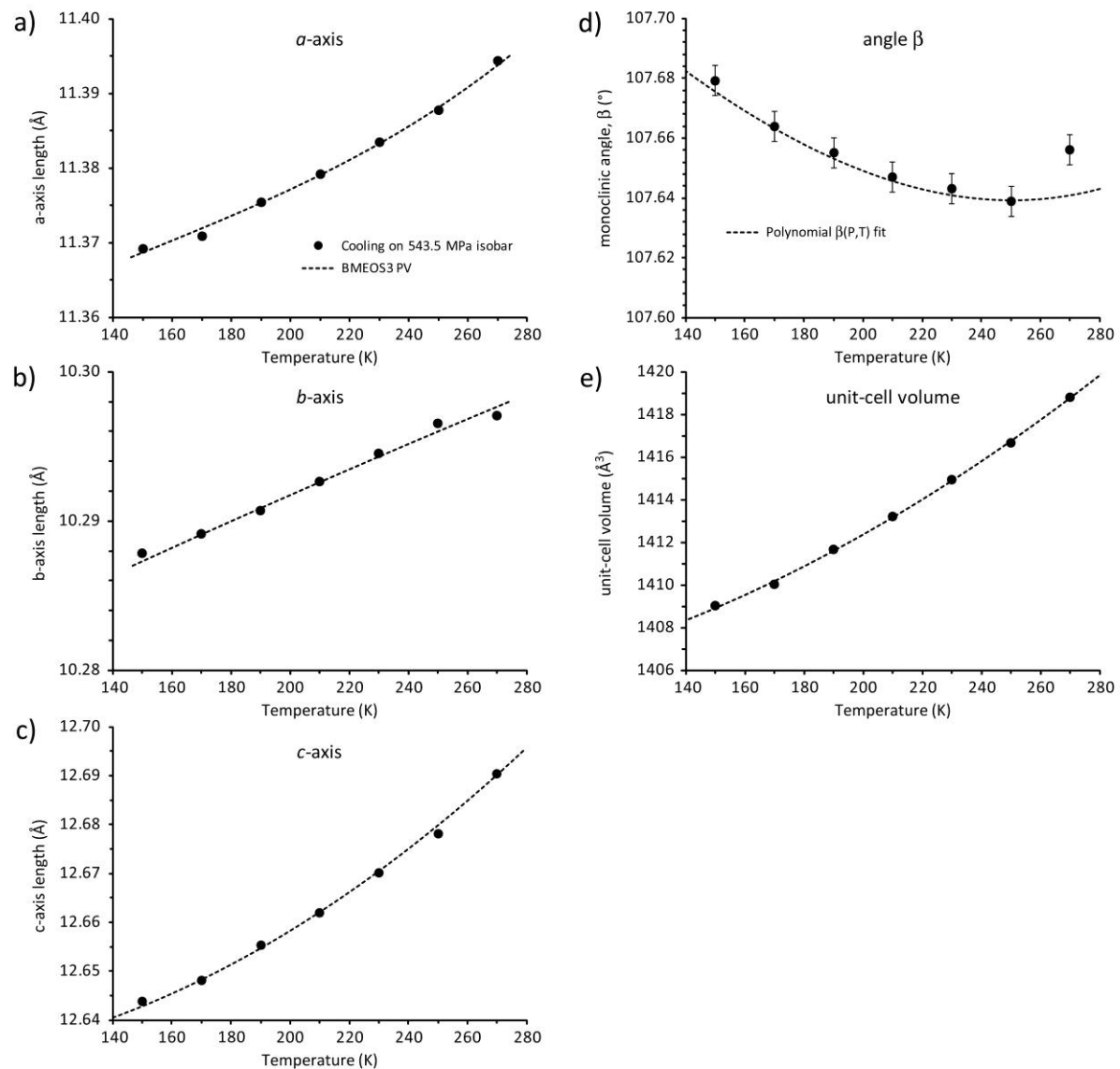


**Figure S3**

Pressure dependence of a) the  $a$ -axis, b) the  $b$ -axis, c) the  $c$ -axis, d) the monoclinic angle  $\beta$  (270 K compression data included for comparison), and e) the unit-cell volume of deuterated mirabilite on decompression at 150 K; dashed lines are isothermal slices through the P-V-T BMEOS3 fitted to the observations. Uncertainties on all observations are smaller than the symbols, with the exception of d) where the error bars depict  $\pm 3\sigma$  uncertainties on  $\beta$ .

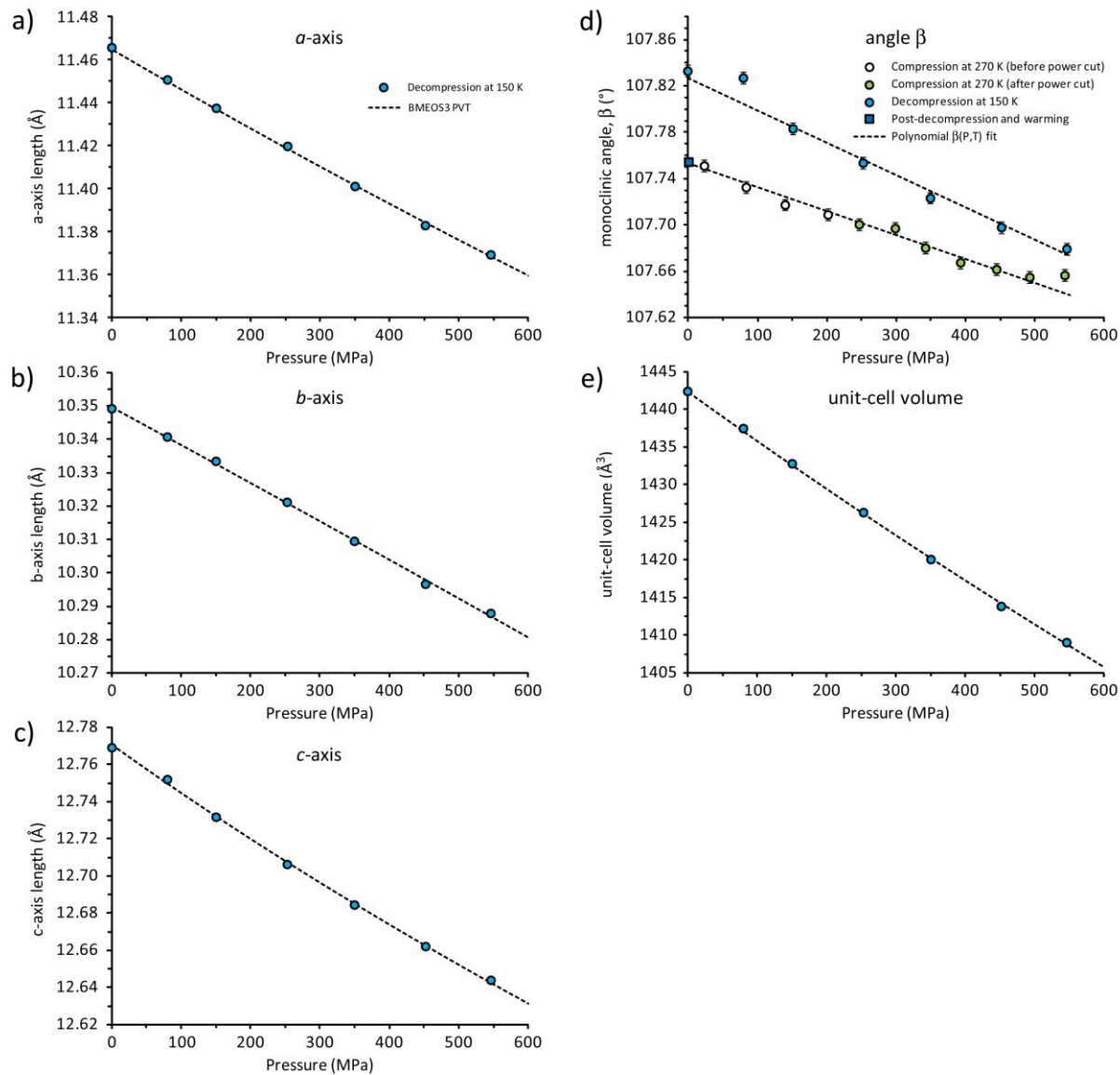


**Figure S4**

(a) Perspective view of the fitted P,T dependence of the  $a$ -axis of deuterated mirabilite; data points are shown as filled circles, red tick marks attached to the data symbols indicate negative misfits, and green tick marks indicate positive misfits. Surface contours are in increments of 50 MPa. Parts (b) and (c) report the relative residuals as a function of temperature and pressure, respectively.

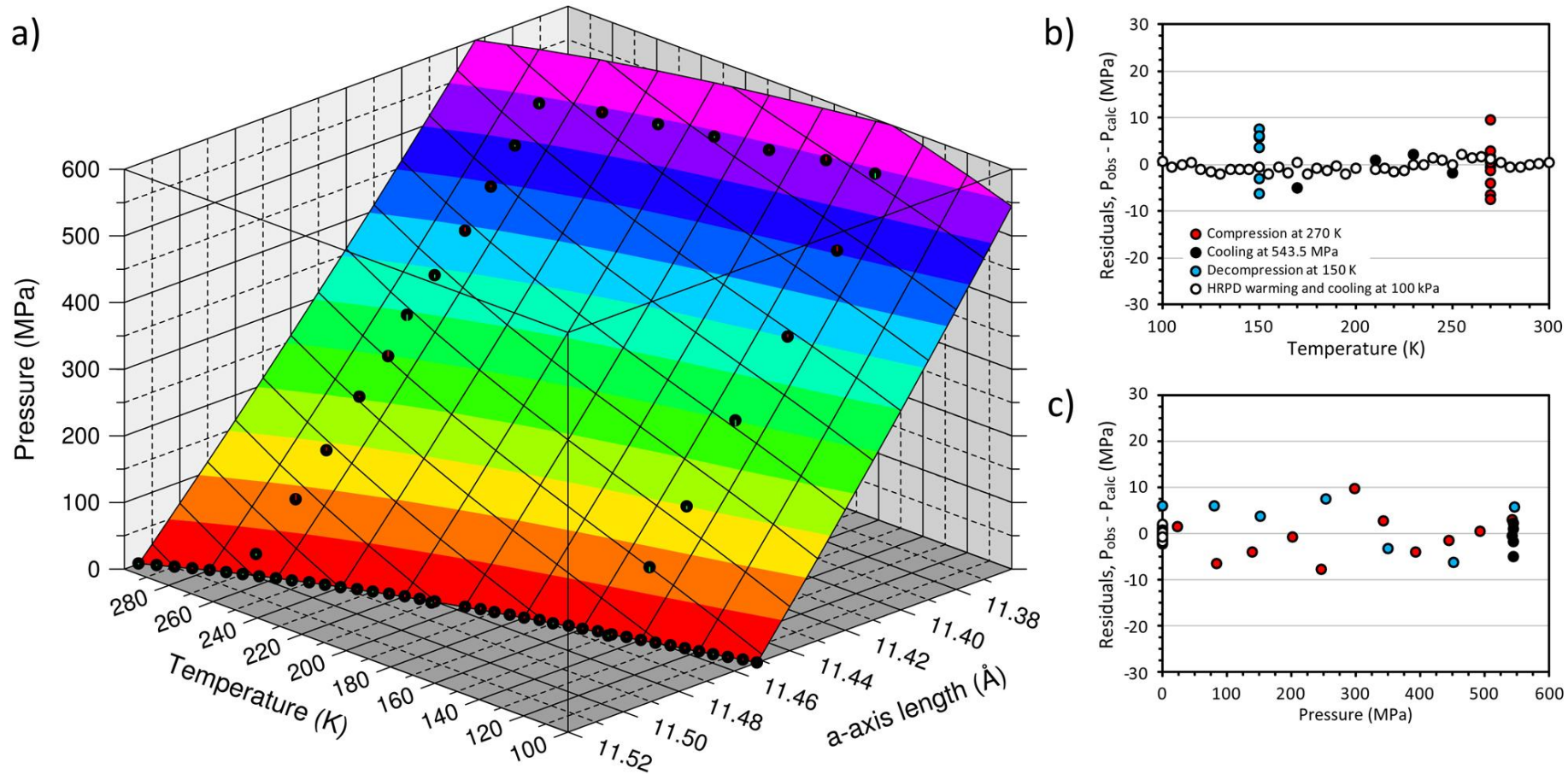


**Figure S5**

(a) Perspective view of the fitted P,T dependence of the *b*-axis of deuterated mirabilite; data points are shown as filled circles, red tick marks attached to the data symbols indicate negative misfits, and green tick marks indicate positive misfits. Surface contours are in increments of 50 MPa. Parts (b) and (c) report the relative residuals as a function of temperature and pressure, respectively.

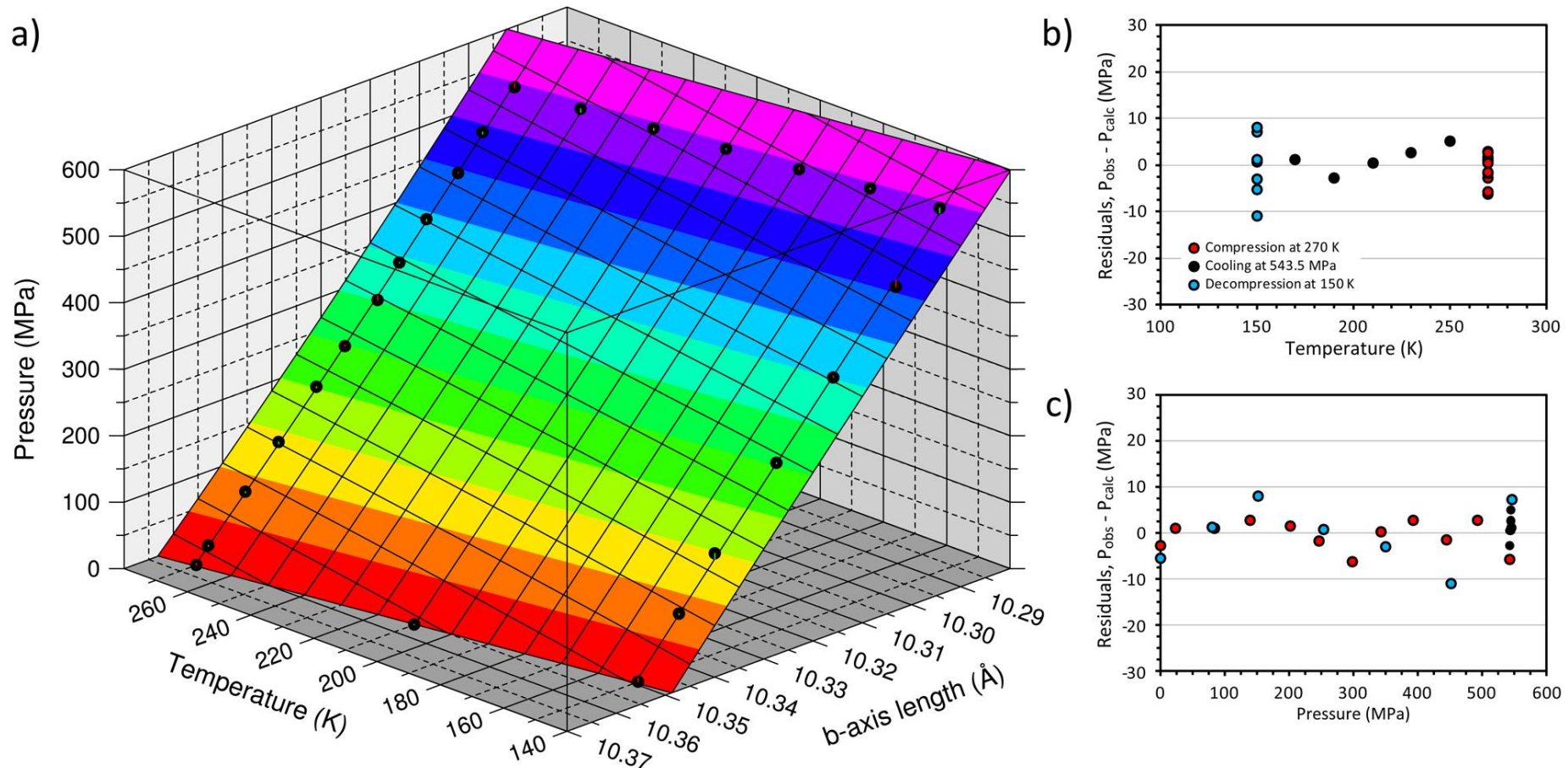


**Figure S6**

(a) Perspective view of the fitted P,T dependence of the *c*-axis of deuterated mirabilite; data points are shown as filled circles, red tick marks attached to the data symbols indicate negative misfits, and green tick marks indicate positive misfits. Surface contours are in increments of 50 MPa. Parts (b) and (c) report the relative residuals as a function of temperature and pressure, respectively. Outlying points discussed in the main text are circled in red.

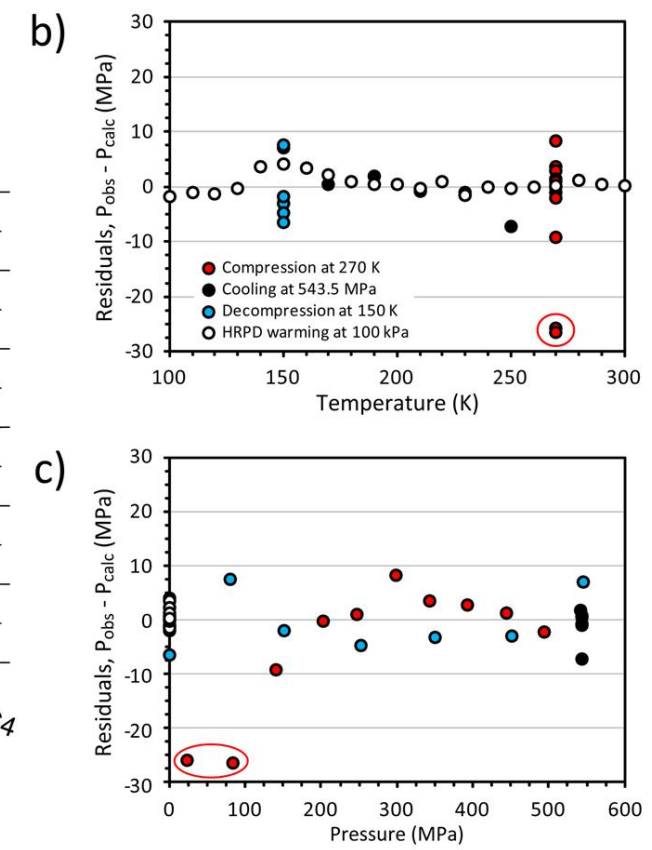
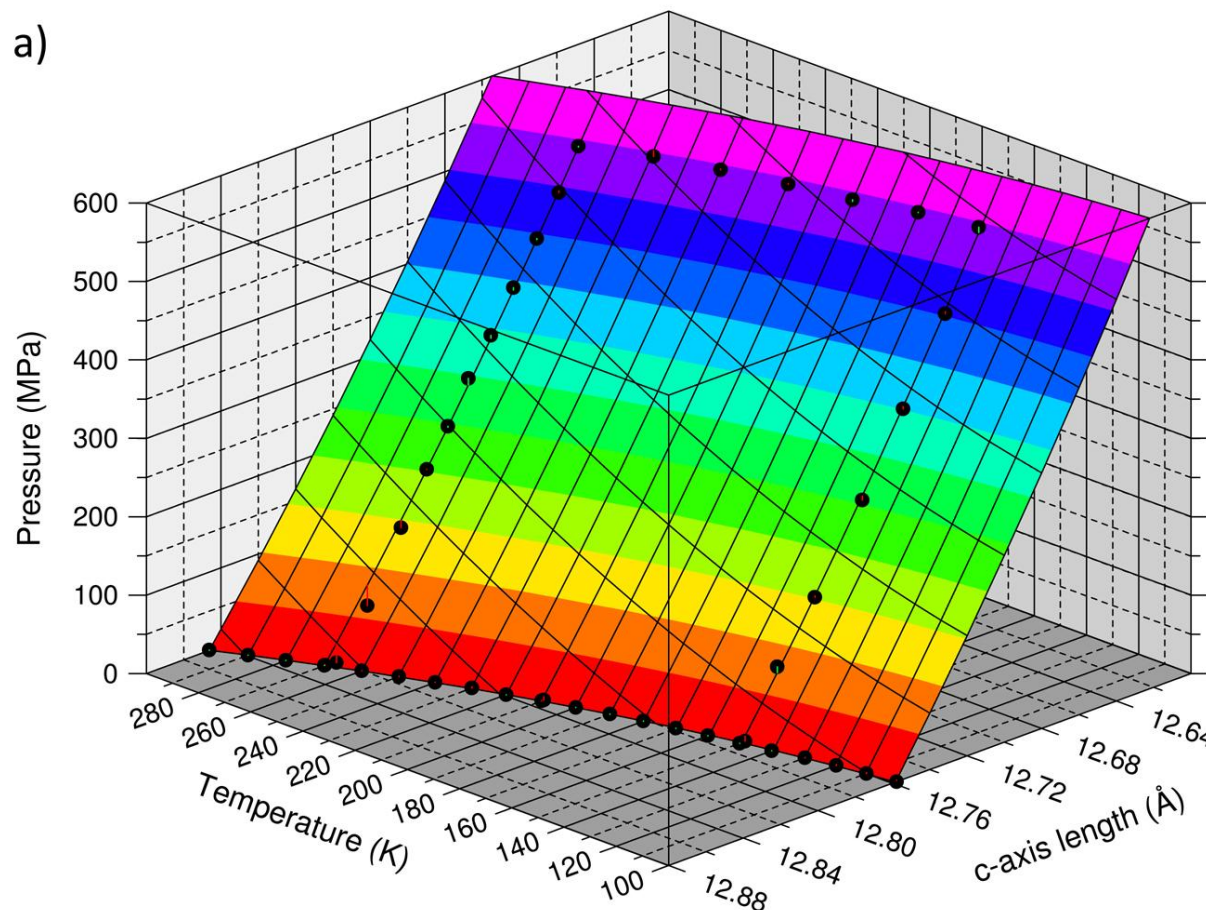


**Figure S7**

a) Perspective view of the fitted P,T dependence of the monoclinic angle  $\beta$  in deuterated mirabilite; data points are shown as filled circles, red tick marks attached to the data symbols indicate negative misfits, and green tick marks indicate positive misfits. Surface contours are in increments of  $0.01^\circ$ . Parts (b) and (c) report the absolute residuals as a function of temperature and pressure, respectively.

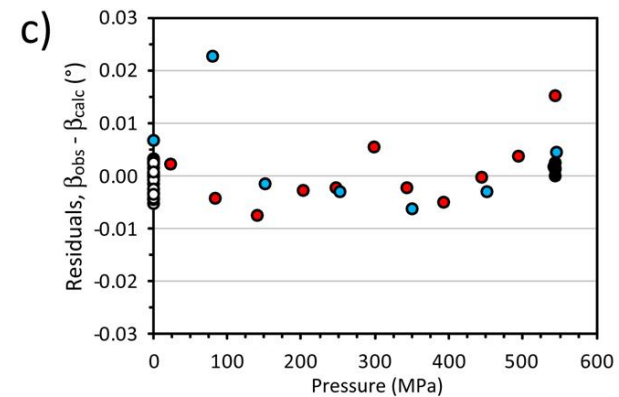
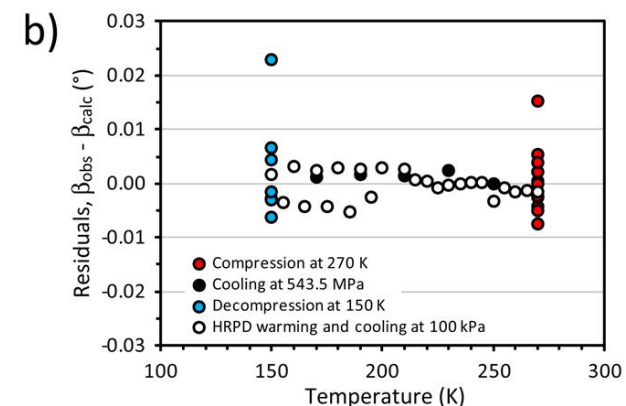
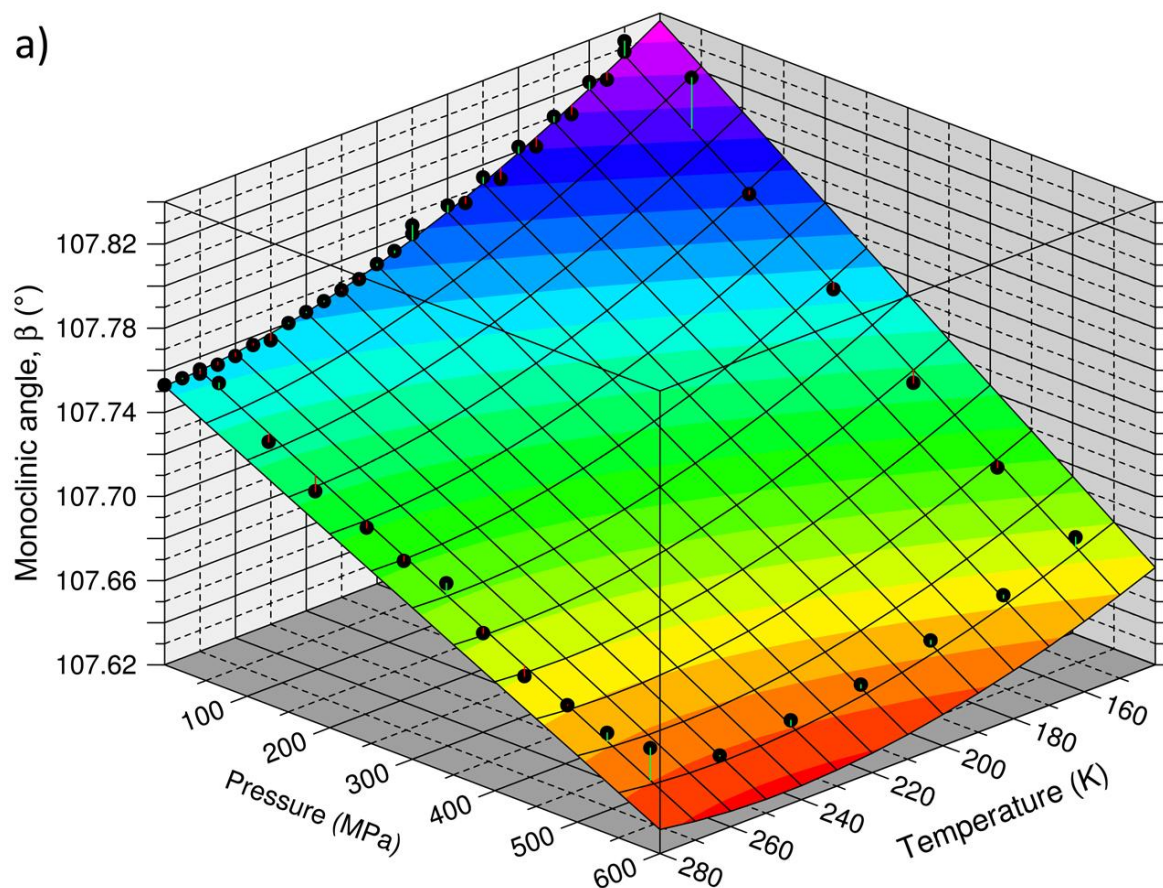


**Figure S8**

(a) Perspective view of the fitted P,T dependence of the direction  $a\sin\beta$  in deuterated mirabilite; data points are shown as filled circles, red tick marks attached to the data symbols indicate negative misfits, and green tick marks indicate positive misfits. Surface contours are in increments of 50 MPa. Parts (b) and (c) report the relative residuals as a function of temperature and pressure, respectively.

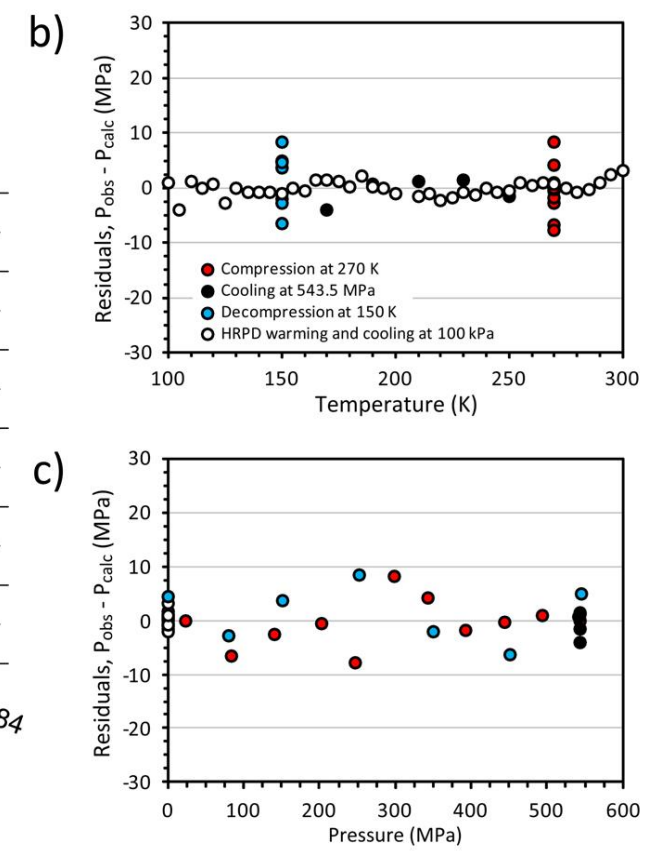
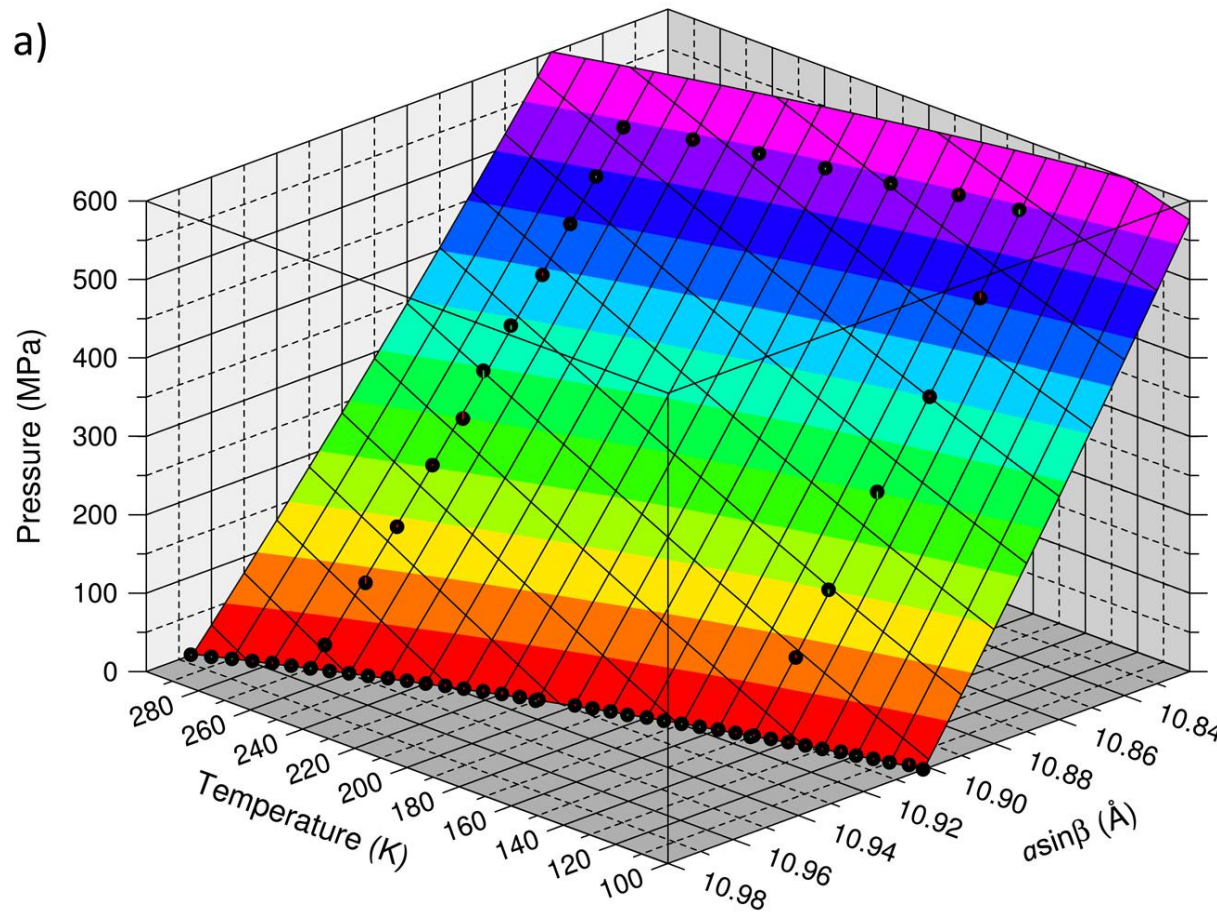


**Figure S9**

Panels a), b), and c) show the pressure dependence of, respectively, the  $a$ -axis, the  $c$ -axis, and the unit-cell volume of deuterated ice IV on decompression at 150 K; dashed lines are Birch-Murnaghan 3<sup>rd</sup> order EOS fits to the observations. Panels d), e), and f) show the temperature dependence of, respectively, the  $a$ -axis,  $c$ -axis, and the unit-cell volume of deuterated ice IV on cooling at 543 MPa. Dashed lines are polynomial functions fitted to the observations.

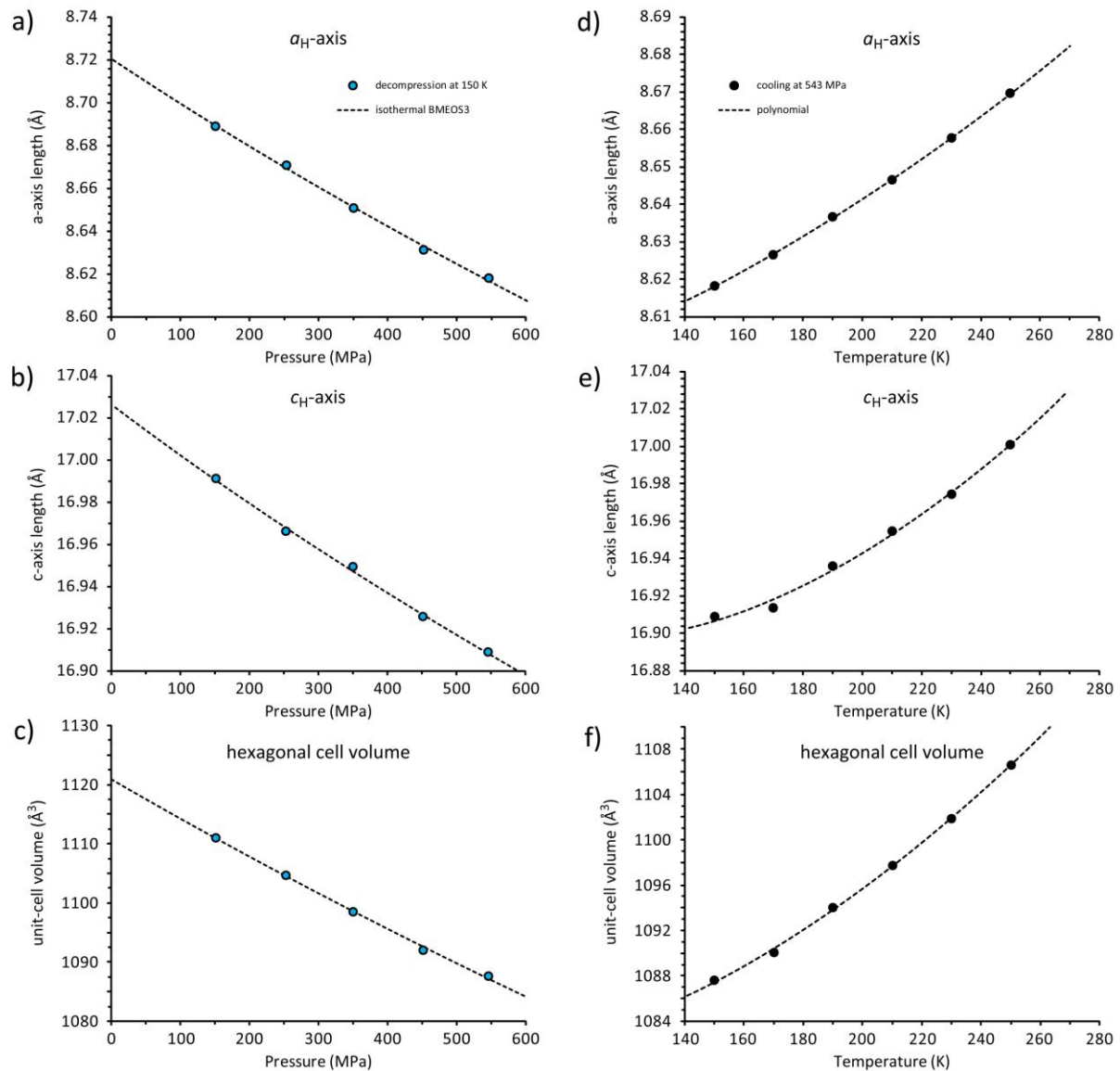


**Figure S10**

Literature data on the high-pressure melting curve of mirabilite (symbols) and a fitted polynomial (dashed line) of the form  $T_m = -4.661 \times 10^{-5} P^2 + 4.923 \times 10^{-3} P + 305.54$  K, where P is in units of MPa.

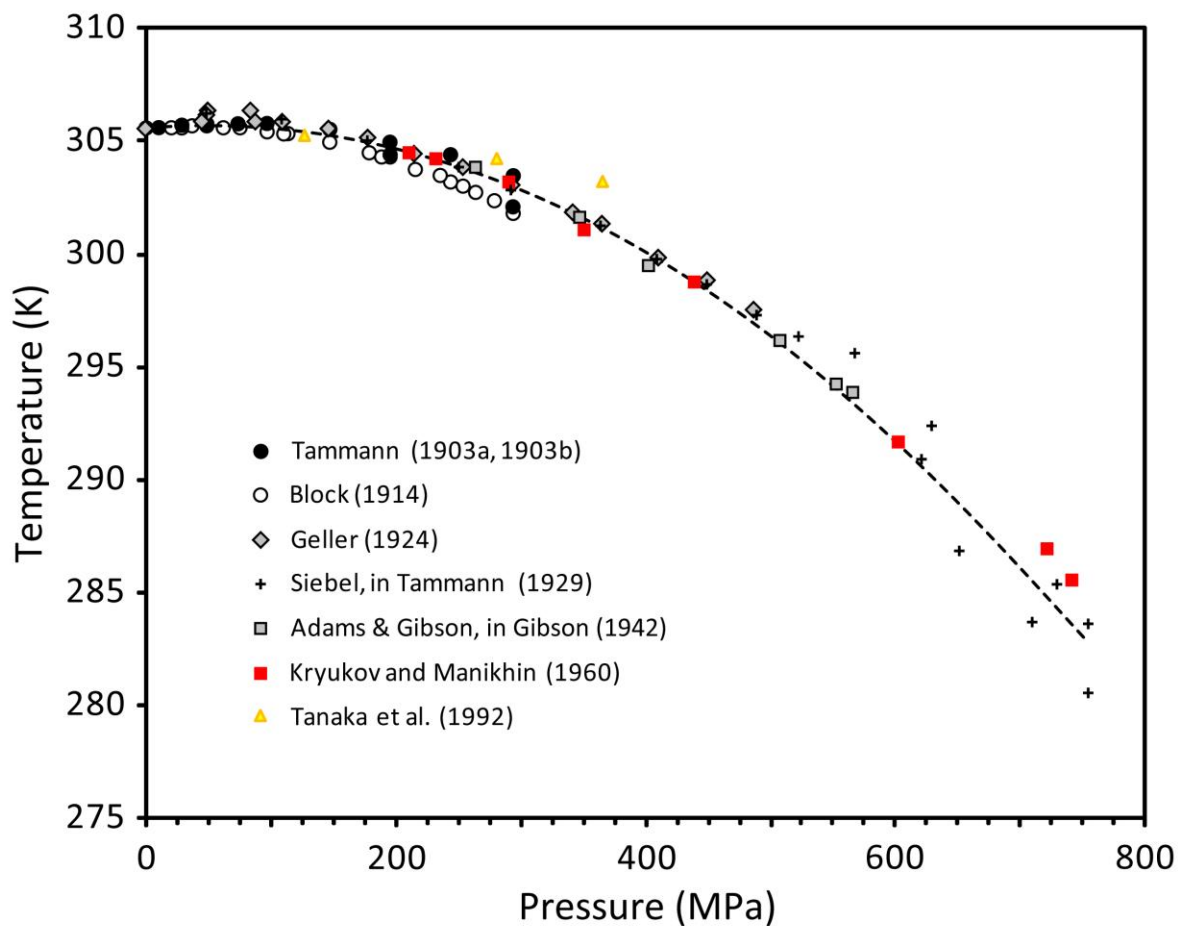


**Table S1**Refined unit-cell parameters of  $\text{Na}_2\text{SO}_4 \cdot 10\text{D}_2\text{O}$  as a function of pressure and temperature.

P (MPa)	T (K)	<i>a</i> (Å)	<i>b</i> (Å)	<i>c</i> (Å)	$\beta$ (°)	V (Å <sup>3</sup> )
23.0	270	11.4965(3)	10.3593(1)	12.8127(2)	107.751(2)	1453.30(3)
83.3	270	11.4822(2)	10.3518(1)	12.7960(2)	107.732(2)	1448.70(3)
139.8	270	11.4711(2)	10.3450(1)	12.7855(2)	107.717(2)	1445.28(3)
202.0	270	11.4592(3)	10.3374(1)	12.7716(2)	107.709(2)	1441.20(3)
253.3	270	<i>Facility power cut during measurement, pressure lost over ca. 6 hr</i>				
247.1	270	11.4488(2)	10.3315(1)	12.7604(2)	107.700(1)	1437.90(2)
298.6	270	11.4421(2)	10.3249(1)	12.7494(2)	107.697(2)	1434.91(3)
343.0	270	11.4321(2)	10.3205(1)	12.7374(2)	107.680(2)	1431.84(3)
393.1	270	11.4212(3)	10.3150(2)	12.7252(2)	107.667(2)	1428.44(3)
445.0	270	11.4118(3)	10.3086(2)	12.7127(2)	107.661(2)	1425.03(3)
493.3	270	11.4031(3)	10.3036(2)	12.7009(2)	107.655(2)	1421.98(3)
543.0	270	11.3944(2)	10.2971(2)	12.6904(2)	107.656(2)	1418.82(3)
544.0	250	11.3877(1)	10.2965(1)	12.6781(2)	107.639(1)	1416.67(2)
544.3	230	11.3835(2)	10.2945(1)	12.6701(1)	107.643(1)	1414.94(2)
543.5	210	11.3792(1)	10.2927(1)	12.6619(1)	107.647(1)	1413.21(2)
542.2	190	11.3755(1)	10.2907(1)	12.6554(1)	107.655(1)	1411.68(2)
544.5	170	11.3709(2)	10.2891(1)	12.6482(1)	107.664(1)	1410.03(2)
546.2	150	11.3692(2)	10.2878(1)	12.6438(1)	107.679(1)	1409.03(2)
451.7	150	11.3829(1)	10.2967(1)	12.6618(1)	107.698(1)	1413.81(2)
349.9	150	11.4008(1)	10.3094(1)	12.6843(1)	107.723(1)	1420.10(2)
253.0	150	11.4196(1)	10.3210(1)	12.7062(1)	107.753(1)	1426.27(2)
150.9	150	11.4372(2)	10.3335(1)	12.7316(1)	107.783(1)	1432.80(2)
80.0	150	11.4506(2)	10.3408(1)	12.7518(1)	107.827(1)	1437.42(2)
0.1	150	11.4655(1)	10.3491(1)	12.7691(1)	107.833(1)	1442.35(2)
0.1	210	11.4812(1)	10.3560(1)	12.7929(1)	107.784(1)	1448.39(2)
0.1	270	11.5013(1)	10.3618(1)	12.8263(1)	107.754(1)	1455.75(2)

**Table S2**

Refined unit-cell parameters of the accessory ice-IV component of the specimen. The refinements were carried out in the triply primitive hexagonal setting; rhombohedral values and uncertainties have been derived from the hexagonal values and uncertainties, and are presented here for completeness and for ready comparison with other work. Primitive rhombohedral unit-cell volumes are one-third of the hexagonal cell volumes,  $V_H$ .

P (MPa)	T (K)	Hexagonal cell				Rhombohedral cell	
		$a_H$ (Å)	$c_H$ (Å)	$V_H$ (Å <sup>3</sup> )	$c_H/a_H$	$a_R$ (Å)	$\alpha$ (°)
544.0	250	8.6696(2)	17.0010(6)	1106.63(4)	1.9610(1)	7.5610(2)	69.963(2)
544.3	230	8.6577(2)	16.9743(6)	1101.86(4)	1.9606(1)	7.5498(2)	69.972(2)
543.5	210	8.6465(2)	16.9547(8)	1097.73(6)	1.9609(1)	7.5406(2)	69.965(2)
542.2	190	8.6368(2)	16.9359(10)	1094.06(7)	1.9609(1)	7.5322(3)	69.965(3)
544.5	170	8.6266(3)	16.9135(13)	1090.05(9)	1.9606(2)	7.5227(3)	69.971(4)
546.2	150	8.6182(2)	16.9091(12)	1087.63(8)	1.9620(2)	7.5184(3)	69.939(4)
451.7	150	8.6312(2)	16.9257(13)	1091.99(8)	1.9610(2)	7.5275(3)	69.963(4)
349.9	150	8.6510(2)	16.9493(10)	1098.53(6)	1.9592(1)	7.5410(3)	70.003(3)
253.0	150	8.6709(3)	16.9664(16)	1104.70(9)	1.9567(2)	7.5528(4)	70.061(4)
150.9	150	8.6890(3)	16.9912(11)	1110.96(7)	1.9555(2)	7.5660(3)	70.090(3)

## References cited

- Block, E. A. (1913): Über die Schmelzkurven einiger Stoffe. *Z. Phys. Chem. Stoichiom. Verwandtschaftse.* **82**, 403-438.
- Geller, A. (1924) Über das verhalten verschiedener minerale der salzlager bei hohen drucken und wechselnden temperaturen. *Z. Krist.* **60**, 415–472.
- Gibson, R. E. (1942) Effect of pressure on phase equilibria in binary condensed systems. In, *Handbook of Physical Constants* (Birch, F., Schairer, J. F., and Spicer, H. C., editors) Geological Society of America Special Papers, No' 36. Geological Society of America, New York, 1942.
- Kryukov, P.A., and Manikhin, V. I. (1960) Characteristics of the melting of Glauber salt at high pressures. *Russ. Chem. Bull.* **9**, 2077-2078 ([doi:10.1007/BF00912067](https://doi.org/10.1007/BF00912067)).
- Tammann, G. (1903a) Die Abhängigkeit des Schmelzepunktes beim Glaubersalz vom Druck. *Z. Phys. Chem.* **64**, 818-826.
- Tammann, G. (1903b) *Kristallisieren und Schmelzen: Ein Beitrage zur Lehre der Änderungen des Aggregatzustandes*. J. A. Barth, Leipzig.
- Tammann, G. (1929) Über die Schmelzkurven einiger Salzhydrate. *Z. Anorg. Allgem. Chem.* **178**, 309-316 ([doi:10.1002/zaac.19291790114](https://doi.org/10.1002/zaac.19291790114)).
- Tanaka, Y., Hada, S., Makita, T. and Moritoki, M. (1992) Effect of pressure on the solid-liquid phase equilibria in (water + sodium sulfate) system. *Fluid Phase Equil.*, **76**(1), 163-173 ([doi:10.1016/0378-3812\(92\)85085-M](https://doi.org/10.1016/0378-3812(92)85085-M)).